

IMPLEMENTATION OF A CATCHMENT  
HYDROLOGIC MODEL FOR THE BRISY  
SUBCATCHMENT OF THE OURTHE  
WATERSHED, AND GENERATION OF A  
DATASET FOR A 240-DAY STORM-INTERSTORM  
SEQUENCE

Rijk Theodoor Oosterhoff and Claudio Paniconi

*Center for Advanced Studies, Research and Development in Sardinia  
(CRS4)  
Cagliari, Italy*

May, 2001

# Contents

<b>List of Figures</b>	<b>3</b>
<b>List of Tables</b>	<b>5</b>
<b>1 Introduction</b>	<b>6</b>
<b>2 Brisby subcatchment</b>	<b>7</b>
<b>3 Data preparation</b>	<b>10</b>
3.1 JRC dataset . . . . .	10
3.1.1 GIS processing . . . . .	11
3.2 KMI dataset . . . . .	13
<b>4 Description of the CATHY model</b>	<b>13</b>
4.1 FLOW3D . . . . .	14
4.2 SURF_ROUTE . . . . .	15
4.3 Algorithm for solving the coupled model . . . . .	16
<b>5 Model setup</b>	<b>16</b>
<b>6 Model simulations</b>	<b>18</b>
6.1 Preliminary simulations . . . . .	18
6.2 Simulation to generate initial conditions . . . . .	19
6.2.1 A note on post-processing . . . . .	19
6.3 240-day storm-interstorm simulation . . . . .	19
<b>7 Conclusions and recommendations</b>	<b>24</b>
<b>References</b>	<b>30</b>

## List of Figures

1	Location of Brisy . . . . .	7
2	Brisy subcatchment . . . . .	8
3	30 x 30 $m^2$ resolution DEM of the Brisy subcatchment, top view . . . . .	8
4	30 x 30 $m^2$ resolution DEM of the Brisy subcatchment . . . . .	9
5	Land cover of the Brisy subcatchment . . . . .	10
6	30 x 30 resolution DEM of the Ourthe Catchment (depitted) . . . . .	12
7	Drainage network (detail) of the Ourthe catchment . . . . .	12
8	Daily rainfall and potential daily evapotranspiration for the selected 240-day period . . . . .	13
9	Location of selected surface nodes for vertical profile output . . . . .	18
10	10-day evaporation simulation: saturation at surface at t=0h . . . . .	19
11	10-day evaporation simulation: saturation at surface at t=240h . . . . .	19
12	10-day evaporation simulation: water saturation at surface at t=240h . . . . .	20
13	10-day evaporation simulation: pressure head (m) at surface nodes t=0h . . . . .	20
14	10-day evaporation simulation: pressure head (m) at surface nodes t=240h . . . . .	20
15	10-day evaporation simulation: water table distribution (m below surface) at t=0h . . . . .	20
16	10-day evaporation simulation: water table distribution (m below surface) at t=96h . . . . .	20
17	10-day evaporation simulation: water table distribution (m below surface) at t=240h . . . . .	20
18	240-day storm-interstorm simulation: saturation at surface at t=0h . . . . .	24
19	240-day storm-interstorm simulation: saturation at surface at t=2160h . . . . .	24
20	240-day storm-interstorm simulation: saturation at surface at t=4321h . . . . .	24
21	240-day storm-interstorm simulation: saturation at surface at t=5760h . . . . .	24
22	240-day storm-interstorm simulation: water saturation at surface at t=0h . . . . .	25
23	240-day storm-interstorm simulation: water saturation at surface at t=2160h . . . . .	25
24	240-day storm-interstorm simulation: water saturation at surface at t=4321h . . . . .	25

25	240-day storm-interstorm simulation: water saturation at surface at t=5760h .	25
26	240-day storm-interstorm simulation: pressure head (m) at surface nodes t=0h	25
27	240-day storm-interstorm simulation: pressure head (m) at surface nodes t=2160h	25
28	240-day storm-interstorm simulation: pressure head (m) at surface nodes t=4321h	26
29	240-day storm-interstorm simulation: pressure head (m) at surface nodes t=5760h	26
30	240-day storm-interstorm simulation: water table distribution (m below surface) at t=0h . . . . .	26
31	240-day storm-interstorm simulation: water table distribution (m below surface) at t=2160h . . . . .	26
32	240-day storm-interstorm simulation: water table distribution (m below surface) at t=4321h . . . . .	26
33	240-day storm-interstorm simulation: water table distribution (m below surface) at t=5760h . . . . .	26
34	240-day storm-interstorm simulation: vertical profile of pressure head at surface node 3295 . . . . .	27
35	240-day storm-interstorm simulation: vertical profile of pressure head at surface node 3315 . . . . .	27
36	240-day storm-interstorm simulation: vertical profile of pressure head at surface node 3331 . . . . .	27
37	240-day storm-interstorm simulation: vertical profile of pressure head at surface node 3337 . . . . .	27
38	240-day storm-interstorm simulation: vertical profile of pressure head at surface node 3341 . . . . .	27
39	240-day storm-interstorm simulation: vertical profile of pressure head at surface node 3347 . . . . .	27
40	240-day storm-interstorm simulation: groundwater velocity (m/h) at t=0h in layer 1 . . . . .	28
41	240-day storm-interstorm simulation: groundwater velocity (m/h) at t=0h in layer 7 . . . . .	28
42	240-day storm-interstorm simulation: groundwater velocity (m/h) at t=5760h in layer 1 . . . . .	29
43	240-day storm-interstorm simulation: groundwater velocity (m/h) at t=5760h in layer 7 . . . . .	29

# List of Tables

1	Soil texture of the Brisq subcatchment in percentages of sand, silt and clay . .	10
2	Soil characteristics of the different layers of the Brisq subcatchment . . . . .	17

# 1 Introduction

This report describes the generation of a synthetic dataset needed for testing and verification of more simplified modeling approaches which aim to develop models applicable at large catchment and river basin scales. The work is carried out within the framework of a European project (DAUFIN) on developing data assimilation methodologies and a unified framework for hydrological modeling of catchment and river basin flow processes. The synthetic dataset will be broadly based on a subset of actual data (topography, geomorphology, and rainfall) for the Brisy subcatchment, which is a subcatchment of the Meuse basin, with representative parameters selected either to "match" equivalent values to be used in the simplified models or to substitute for any input data which is currently unavailable. The simulated dataset to be generated will encompass both rainfall and interstorm periods and a variety of rainfall-runoff responses (both surface and subsurface). The simulation outputs of interest include pressure heads, groundwater fluxes, and water table and surface soil moisture (or saturation) distributions.

A catchment partitions atmospheric forcing (rainfall and potential evaporation) into surface runoff, groundwater flow, actual evapotranspiration, and changes in storage. Surface runoff involves different phenomena such as hillslope and channel flow and retardation and storage effects due to pools and lakes, while groundwater flow includes infiltration to and exfiltration from the vadose zone. The numerical model to be used in this work, CATHY (CATchment HYdrological model), simulates these various processes based on a coupling of the Richards equation for variably saturated porous media and a diffusion wave approximation for surface water dynamics. It combines a 3D finite element subsurface flow module, FLOW3D, with a 1D finite difference surface routing module, SURF\_ROUTE. Hillslope flow is assumed to concentrate in rills or rivulets, allowing both channel and hillslope flow to be described by a 1D convection-diffusion equation. Retardation and storage effects due to lakes or depressions are also implemented, giving a complete description of the catchment flow dynamics. The model's basic inputs are a DEM (digital elevation model) from which discretization of the catchment surface and a corresponding 3D grid of the underlying aquifer are obtained, atmospheric fluxes (rainfall and evaporation), and various soil, channel, and aquifer parameters.

The objective of this study is to adapt and implement the existing model (CATHY) to a dataset broadly based on the Brisy subcatchment and to generate simulation datasets that will:

- shed light on the numerical and physical behavior of the model in capturing various hydrological flow responses;
- be used for objectively testing the hypotheses and limitations of more simplified modeling approaches.
- be used for testing data assimilation (eg, nudging) methodologies

The following workplan is carried out:

- Data preparation (organize and process available data of Meuse basin and Brisy subcatchment, and define appropriate values or ranges of values for parameters);



Figure 1: Location of Brisy

- Implementation (adapt and implement the model for the selected input dataset, and run preliminary tests to examine how the model responds to different parameter settings);
- Simulation (final selection of the scenarios to be run and generation of the synthetic dataset based on these scenarios);
- Analysis (examine the simulation results to assess model performance and to produce the outputs and summary statistics of interest in verifying simplified approaches).

## 2 Brisy subcatchment

Near the northwestern border of Luxembourg runs the Ourthe Orientale from east to west. From south to north runs the Ourthe Occidentale, a watershed of the Meuse basin (Figure 1). Where they meet, near the town of Engreux, they form the Ourthe which flows northwards and eventually drains into the river Meuse. Approximately 10 - 15 kilometers east of the point where the Ourthe Orientale meets the Ourthe Occidentale, near the town of Brisy, flows the river Brisy from north to south into the Ourthe Orientale.

The Brisy subcatchment (Figures 2 and 3) encompasses an area of 4.64 square kilometers (maximum length: 2.85 km from east to west and 3.27 km from north to south). The subcatchment contains shallow slopes in the north and steeper slopes in the south, towards the outlet of the catchment (see Figure 4).

Figure 5 is a map of the land cover of the Brisy subcatchment. The part indicated as “discon-



Figure 2: Brisy subcatchment

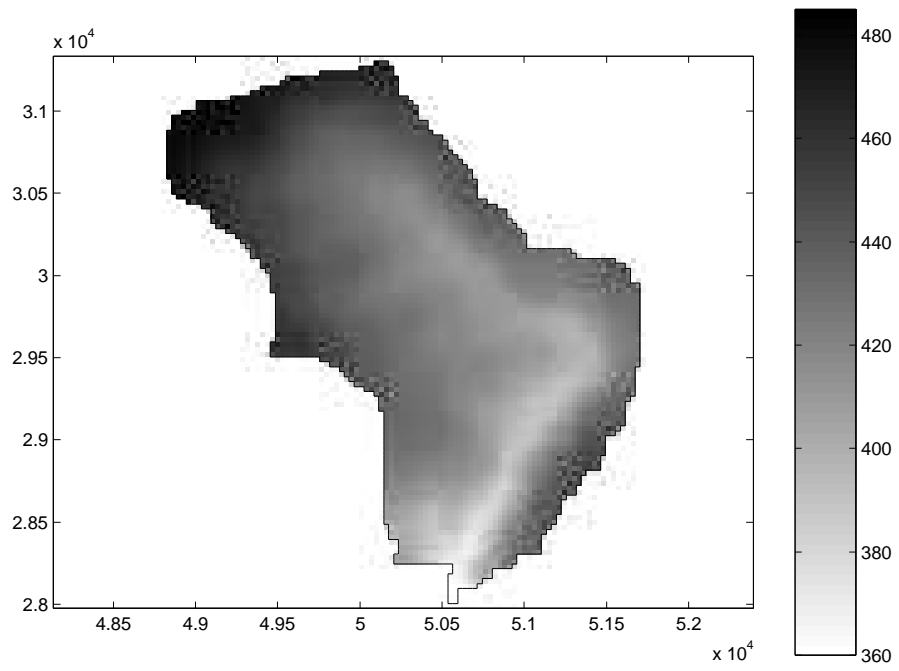


Figure 3:  $30 \times 30 \text{ m}^2$  resolution DEM of the Brisy subcatchment, top view



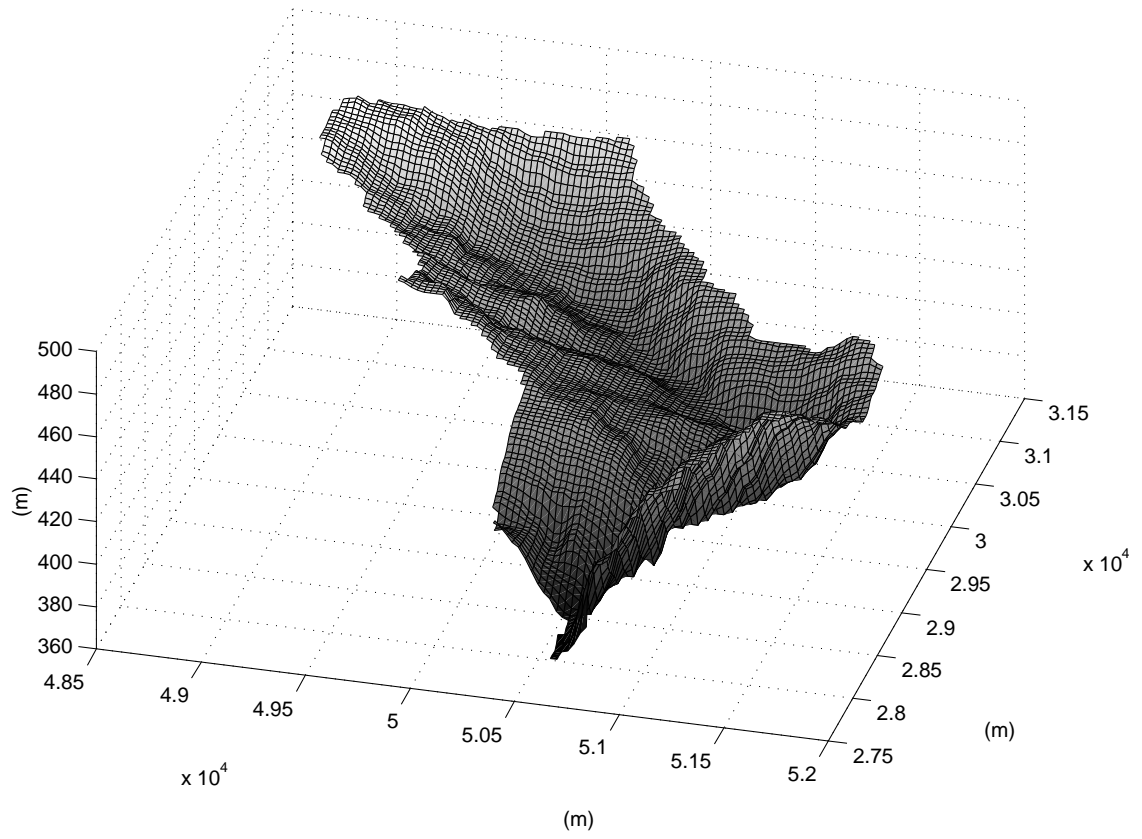


Figure 4:  $30 \times 30 \text{ m}^2$  resolution DEM of the Brisy subcatchment

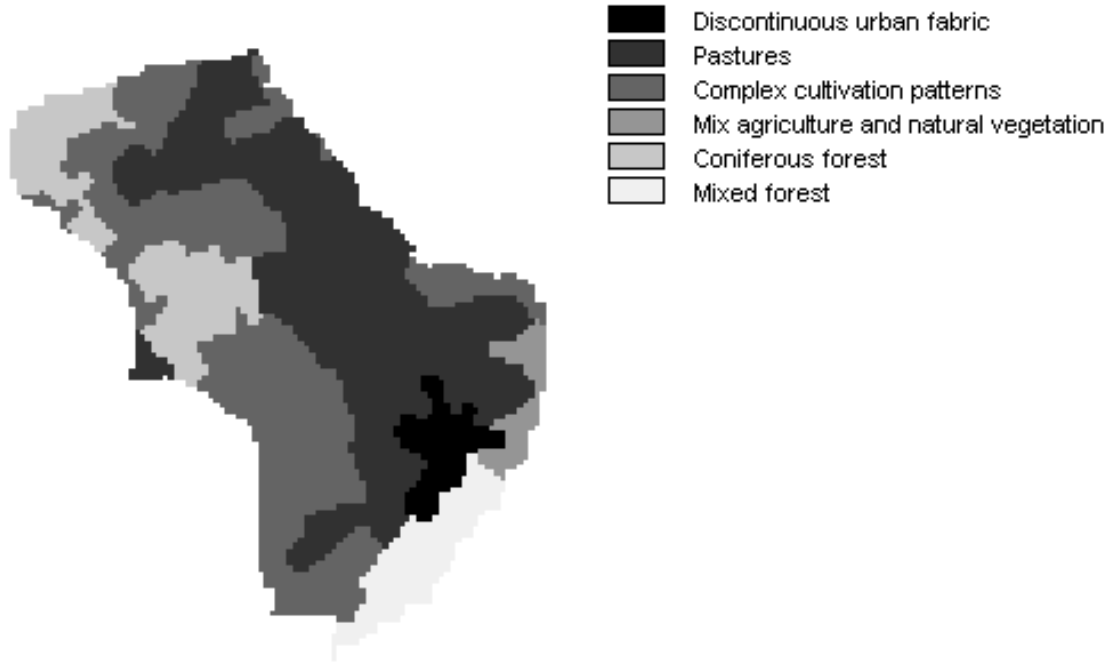


Figure 5: Land cover of the Brisys subcatchment

Table 1: Soil texture of the Brisys subcatchment in percentages of sand, silt and clay

	Topsoil	Subsoil
Sand	33.9	6.6
Silt	47.0	46.4
Clay	19.1	47.0

tinuous urban fabric” is the town of Brisys. Besides the town of Brisys and a few parts covered with forest, most of the catchment is covered with pastures and fields.

The soil of the catchment is approximately 3.0 m thick. The texture of the topsoil differs somewhat from the texture of the subsoil. Table 1 gives the percentages of sand, silt and clay in the topsoil and the subsoil.

### 3 Data preparation

#### 3.1 JRC dataset

The data for the Brisys subcatchment was extracted from 2 datasets of the Meuse basin (Ourthe and Geer watersheds) prepared for the DAUFIN project by the Joint Research Center (JRC)

[*de Roo and Somma* 2000] and by the Belgium Royal Meteorological Institute (KMI) [*Roulin* 2000].

#### DEM data

The original data for the DEM is provided by the Belgian National Geographic Institute in geographic projection (datum wgs84) with a resolution (lat.  $\times$  lon.) of 1"  $\times$  1" below 50° N (2 maps, 15"  $\times$  15" block) and of 2"  $\times$  2" above 50° N (18 maps, 15"  $\times$  15" block). Blocks have been resampled to 30  $\times$  30 meter grid and merged to a single map.

#### Land cover data

Original data from CORINE database provided by European Topic Centre at Satellus AB, Kiruna - Sweden, in Lambert Azimuthal projection with a resolution of 250 m.

#### Soil depth

Original data is provided by European Soil Bureau, Joint Research Centre, Ispra - Italy, in Lambert Azimuthal projection at a scale of 1:1,000,000.

#### Soil texture for top- and subsoil

Original data is provided by European Soil Bureau, Joint Research Center, ISP - Italy, in Lambert Azimuth projection at the scale of 1:1,000,000.

### **3.1.1 GIS processing**

All data is provided in ArcView / ArcInfo ASCII raster files. Using the function SSTIDRIS the data is imported into the IDRISI geographic information system (GIS). This function uses the row and column structure of the ASCII file as a direct analogue of the row and column structure of an image. SSTIDRIS reads the ASCII file and converts it into an IDRISI image. Further GIS processing is done in IDRISI.

To avoid problems due to local depressions in the DEM (pits) the function PIT REMOVAL is applied to the DEM. The purpose of this module is to create an adjusted "depressionless" DEM (Figure 6) in which the cells contained in depressions are raised to the lowest elevation value on the rim of the depression. Each cell in the depressionless DEM will then be part of a monotonically decreasing path of cells leading to an edge of the image. A path is composed of cells that are adjacent horizontally, vertically, or diagonally in the raster grid and that steadily decrease in value.

From the DEM a map of the drainage network is created using the function RUNOFF. RUNOFF calculates the accumulation of rainfall units per pixel as if one unit of rainfall was dropped on every location. Using the RECLASS module, a threshold value of 511 is applied to the output to produce the drainage network (Figure 7).

To identify the subcatchment the function WATERSHED is applied to the DEM. WATERSHED identifies watersheds from a raster surface image. A seed image is provided with the seed located in the stream right before the Brisy enters the Ourthe Orientale.

Working from this map of the Brisy subcatchment, maps of land cover, soil depth, and soil

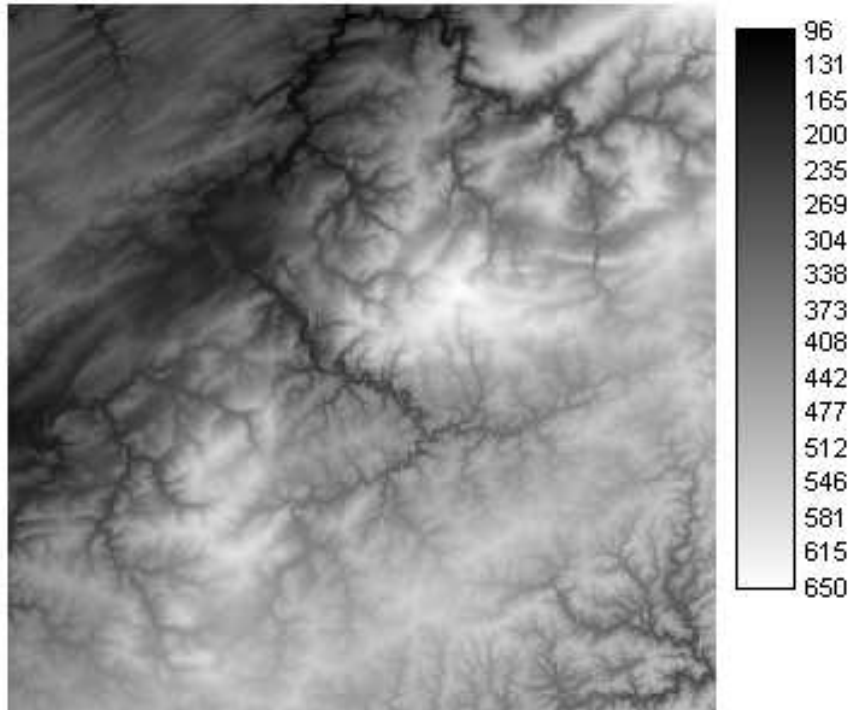


Figure 6: 30 x 30 resolution DEM of the Ourthe Catchment (depitted)

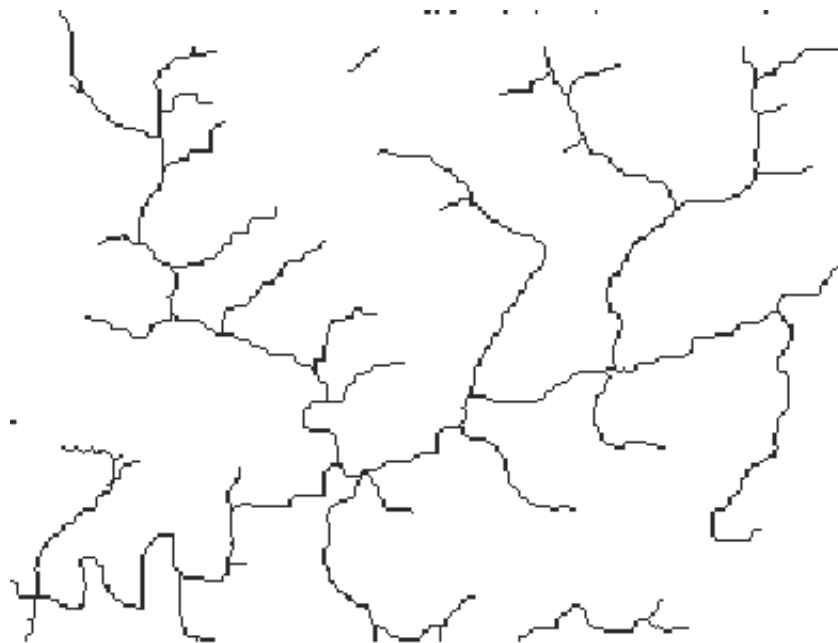


Figure 7: Drainage network (detail) of the Ourthe catchment

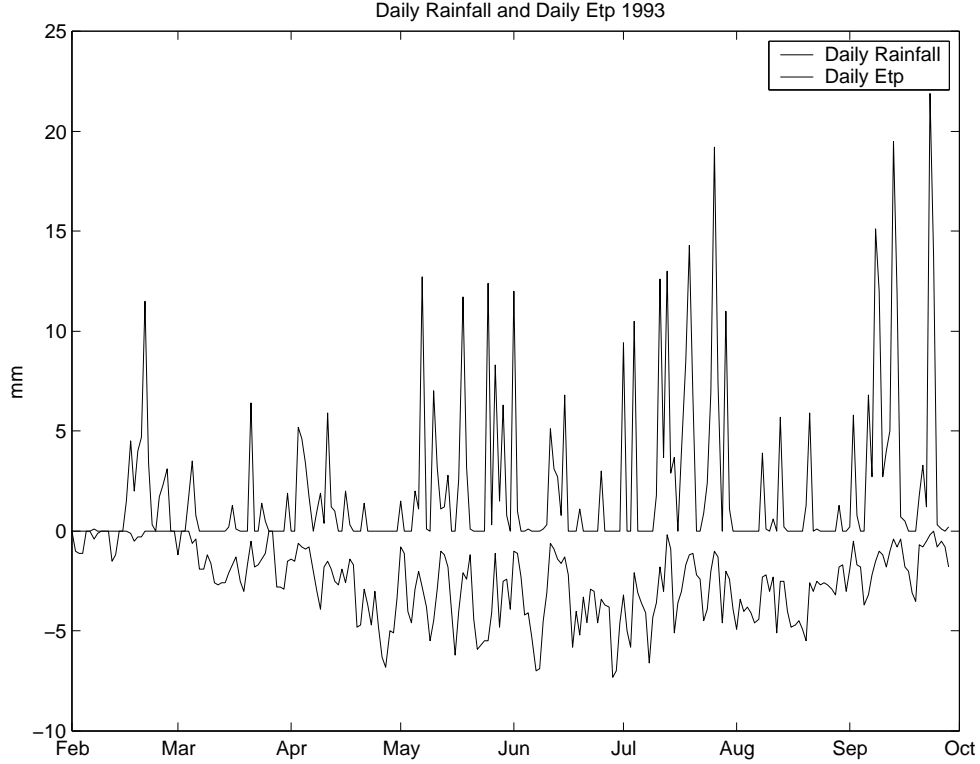


Figure 8: Daily rainfall and potential daily evapotranspiration for the selected 240-day period

texture are created for the catchment using the IMAGE CALCULATOR in IDRISI. According to the JRC dataset, soil depth and soil texture is fairly homogeneous over the Brisys subcatchment.

### 3.2 KMI dataset

The KMI dataset contains meteorological data recorded at several stations on the Ourthe and Geer watersheds. For this study data of rainfall and evapotranspiration for the meteorological station in St. Hubert is used. This station is located 15 to 20 kilometers southwest of the Brisys subcatchment. For the period 1968 to 1997 files containing daily rainfall (mm/day) and (potential) daily evapotranspiration (mm/day) are provided.

Plots of rainfall (mm/10 days) and potential evapotranspiration (mm/10 days) are created. From these plots the 8-month period from February to October 1993 (240 days) is selected (Figure 8). To get the net atmospheric flux needed for input to the CATHY model the potential daily evapotranspiration is subtracted from the daily rainfall and converted to m/hour.

## 4 Description of the CATHY model

The CATHY model is a physically-based distributed catchment-scale model for the simulation of coupled surface runoff and subsurface flow [Bixio *et al.* 2000]. The model is based on coupling Richard's equation for variably saturated porous media and a diffusion wave approx-

imation for surface water dynamics. The numerical scheme uses a finite element Richards' equation solver, FLOW3D [Paniconi and Wood 1993; Paniconi and Putti 1994] and a surface DEM-based finite difference module, SURF\_ROUTE [Orlandini and Rosso 1996]. Starting from a DEM discretization of the catchment surface and an aquifer, atmospheric input is partitioned into surface and subsurface components by the FLOW3D module. The overland flux values calculated by FLOW3D at the grid nodes are transferred to the DEM cells and implemented as sink or source terms in the SURF\_ROUTE module, which routes this surface water and calculates the resulting ponding head values that are in turn used as boundary conditions in FLOW3D.

The model is based on a system of two partial differential equations, one describing the flow of water in the vadose and groundwater zone (Richards' equation) and the other describing the surface hydrologic response of the catchment. The assumption is made that hillslope flow concentrates in rills or rivulets. Hence both channel and hillslope flow can be described by a one dimensional convection-diffusion equation defined on the rill or channel network using different parameter values to distinguish between both types of flow. The system of partial differential equations is:

$$\sigma(S_w) \frac{\partial \psi}{\partial t} = \nabla \cdot [K_s K_{rw}(S_w) (\nabla \psi + \eta_z)] + q_s(h) \quad (1)$$

$$\frac{\partial Q}{\partial t} = c_k \frac{\partial Q}{\partial t} = D_h \frac{\partial^2 Q}{\partial s^2} + c_k q_L(h, \psi) \quad (2)$$

Where  $\sigma(S_w) = S_w S_s + \phi \frac{\partial S_w}{\partial \psi}$ ,  $S_w$  is water saturation,  $S_s$  is the aquifer specific storage coefficient,  $\phi$  is porosity,  $\psi$  is pressure head,  $t$  is time,  $\nabla$  is the gradient operator,  $K_s$  is the saturated hydraulic conductivity,  $K_{rw}$  is the relative hydraulic conductivity,  $\eta_z = (0, 0, 1)^T$ ,  $z$  is the vertical coordinate director upward, and  $q_s$  represents distributed source or sink terms (volumetric flow rate per unit volume). The surface water is routed using (2) along each single hillslope or channel using a one-dimensional coordinate system  $s$  defined on the drainage network. In this equation,  $Q$  is the discharge along the channel link,  $c_k$  is the kinematic wave celerity,  $D_h$  is the hydraulic diffusivity, and  $q_L$  is the inflow (positive) or outflow (negative) rate from the subsurface into the cell. Note that  $q_s$  and  $q_L$  are both functions of the ponding head  $h$ , and that  $h$  can be easily derived from the discharge  $Q$  via mass balance calculations. This system of equations must be solved simultaneously for the unknowns  $(Q, \psi)$  or  $(h, \psi)$ . Nonlinearities arise in the  $S_w(\psi)$  and  $K_{rw}(S_w)$  characteristic curves in Richards' equation, in the nonlinear dependence of  $q_s$  on the ponding head, and in the nonlinear dependence of  $q_L$  on  $\psi$ .

#### 4.1 FLOW3D

FLOW3D is a three-dimensional finite element model for flow in variably saturated porous media, applicable to both the unsaturated and saturated zones. Equation (1) is highly nonlinear due to pressure head dependencies in the storage and conductivity terms, and is linearized in the code. Tetrahedral elements and linear basis functions are used for the discretization in space, and a weighted difference scheme is used for the discretization in time. The input

flux for the atmospheric boundary conditions are potential rainfall or evaporation rates. The actual rates, which depend on the prevailing flux and pressure head values at the surface, are dynamically calculated by the code during the simulation.

Overland flow, which is the flow rate that is present at the surface and that can be routed via the surface model, is calculated at every time step from the balance between potential and actual fluxes. Automatic switching of surface boundary conditions from a specified flux (Neumann) to a constant head (Dirichlet) condition, and vice versa, is implemented to correctly reproduce the physical phenomena occurring at the surface. If a surface node becomes saturated because the water table reaches the surface and there is an upward flux across the soil surface, the overland flow is calculated as the sum of precipitation and return flux. The amount of water that remains at the surface or exfiltrates from the subsurface is then transferred for routing to the DEM-based surface runoff module, which in turn returns, after surface propagation, the ponding head distribution to FLOW3D.

## 4.2 SURF\_ROUTE

Hillslope flow is assumed to concentrate in rills or rivulets that form because of topographic irregularities or differences in soil erodability and that deepen and widen during the runoff event as a function of slope, runoff characteristics and soil erodability. To minimize the computational effort and economize on the number of model parameters, the rill formations are lumped at the DEM elemental scale into a single conceptual channel. The drainage system topography and compositions are described by extracting automatically a conceptual drainage network from the DEM. Each elemental hillslope rill and network channel is assumed to have bed slope and length that depend on location within the extracted transport network, and a rectangular cross section whose width varies dynamically with discharge according to the scaling properties of stream geometry as described by the "at-a-station" and "downstream" relationships [Leopold and Maddock Jr. 1953]. The distinction between hillslope and channel flow is based on the "constant critical support area" concept [Montgomery and Foufoula-Georgiou 1993]. Rill flow is assumed to occur for all those cells for which the upstream drainage area  $A$  does not exceed the constant threshold value  $A^*$ , while channel flow is assumed to occur for all those cells for which  $A$  equals or exceeds  $A^*$ .

A routing scheme developed on the basis of the Muskingum-Cunge method with variable parameters is used to describe both hillslope rill and network channel flows, with different distributions of the Gauckler-Strickler roughness coefficients to take into account the different processes that characterize the two physical phenomena [Orlandini and Rosso 1998]. The model routes surface runoff downstream from the uppermost DEM cell in the basin to the outlet, following the previously determined drainage network. A given grid cell will receive water from its upslope neighbor and discharge it to its downslope neighbor, with the inflow or outflow rate  $q_L$  at any catchment cell given by:  $q_L = q \frac{\Delta x \Delta y}{\Delta s}$ , where  $q$  is the local contribution to surface runoff, as calculated by FLOW3D,  $\Delta x$  and  $\Delta y$  are the cell sizes, and  $\Delta s$  is the channel length within the cell. Inflow hydrographs and overland fluxes  $q_L$  are routed into each individual channel via the convection-diffusion flow equation (2), discretized by the Muskingum-Cunge method to yield:

$$Q_{i+1}^{k+1} = C_1 Q_i^{k+1} + C_2 Q_i^k + C_3 Q_{i+1}^k + C_4 q_{L,i+1}^k \quad (3)$$

where  $Q_{i+1}^{k+1}$  is discharge at network point  $(i+1)\Delta s$  and time  $(k+1)\Delta t$ ,  $q_{kL_{i+1}}$  is the overland flow rate at the  $(i+1)$ st space interval and time  $k\Delta t$ , and the routing coefficients  $C_i$  depend on  $c_k$ , on the temporal interval  $\Delta t$ , on the channel length  $\Delta s$ , and on the numerical scheme. Once the in and out discharge at each cell is determined, the cell water depth, or ponding head  $h$ , can be calculated from mass balance considerations. The distinction if a surface node is saturated or ponded is made via the input parameter `pond_h_min`. This is the threshold pressure head value that a surface node must attain to be considered ponded.

### 4.3 Algorithm for solving the coupled model

For every timestep the following algorithm is followed to solve the coupled system (1) and (2):

- Solve (2) using  $q_L^k$  as input to the SURF\_ROUTE model, obtaining  $Q^{k+1}$  and from this the distribution of ponding heads  $h^{k+1}$ .
- Use  $h^{k+1}$  and precipitation/evaporation input at time  $t^{k+1}$  to set up boundary and initial conditions for FLOW3D, and solve (1) for  $\psi^{k+1}$ .
- Calculate (again with FLOW3D) the overland flux  $q_L^{k+1}$  using  $\psi^{k+1}$  and the balance between atmospheric inputs and actual fluxes.

Note that to start the algorithm a initial value for  $q_L$  is needed. If this condition is not known it can be calculated from an initial run of FLOW3D that will evaluate a first guess for the overland flow based on the actual atmospheric input.

## 5 Model setup

The input data for the CATHY model is structured in the following input files:

**Parm** Numerical, time, and output control parameters for FLOW3D and SURF\_ROUTE.

**Grid** Triangular grid info. Empty when a DEM is used as input and a triangular grid is generated from this DEM.

**Nansfnodbc** Non-atmospheric, non-seepage face nodes with Neumann or Dirichlet boundary conditions (BCs).

**Soil** Soil characteristics (saturated hydraulic conductivity, specific storage and porosity) and parameter values for the unsaturated zone characteristic relationships (van Genuchten, Huyakorn or Brooks-Corey curves).

**Ic** Initial conditions.

**Atmbc** Atmospheric BCs (rainfall/evaporation rates, imported as histograms).

**Sfbc** Seepage face BCs.

**Nansfdirbc** Non-atmospheric, non-seepage face Dirichlet BC values.



Table 2: Soil characteristics of the different layers of the Brisy subcatchment

Layer	$K_s$ (m/day)	Specific Storage( $m^{-1}$ )	Porosity	Thickness (m)
1	2.5 e-2	0.016	0.45	0.27
2	2.5 e-2	0.016	0.45	0.36
3	2.5 e-2	0.016	0.45	0.39
4	3.71 e-3	0.016	0.49	0.66
5	3.71 e-3	0.016	0.49	0.66
6	3.71 e-3	0.016	0.49	0.66

**Nansfneubc** Non-atmospheric, non-seepage face Neumann BC values.

**Dembrisy.dat** DEM information. In this study the DEM of the Brisy subcatchment.

**Dem\_parameters.dat** DEM parameters that determine the way in which the CATHY model generates a triangular grid from the DEM.

**Geometry.dat** Geometry characteristics of the surface routing network (threshold for partitioning between channel and hillslope nodes, channel and rill geometry parameters, Leopold and Maddock coefficients).

**Ks.dat** Gauckler-Strickler roughness coefficients  $k_s$  ( $k_s = 1/n$  where  $n$  is the Manning coefficient)

**Force\_flowdir.dat** Cells with imposed (or forced) drainage direction.

**Force\_hg.dat** Cells with imposed (or forced) flow geometry.

**Posizione\_serb.dat** Position of reservoirs (e.g. lakes) and associated buffer cells.

**Livelli\_iniz\_s.dat** Initial water levels in reservoirs.

**Depit.dat** Depitting tolerance parameter.

**Lakes\_map.dat** Map of reservoir or lake cells.

For the simulations the threshold value `pond_h_min` for distinguishing between saturation and ponding was set to 0.01 m. No stream channels were predefined (a high value for the constant critical support area  $A^*$  was used, implying only hillslope or rill overland flow). No lakes or reservoirs were discretized on the subcatchment, and no seepage face and non-atmospheric/non-seepage face boundary conditions were used. Literature values were used for the Leopold-Maddock and Gauckler-Strickler coefficients. According to the JRC dataset the soil depth is about 3 m. This soil depth was divided into 6 layers with different characteristics for the topmost and bottommost 3 layers (Table 2). The vertical discretization of the subcatchment was made such that each layer is parallel to the surface, including the base of the 3D grid. The maximum time step used in the simulations was 2.0 hours, adequate for capturing flow processes generated by daily-averaged inputs of evaporation and rainfall.

For the Brisy subcatchment 6 surface nodes were selected for vertical profile output. Figure 9 shows the locations of these selected surface nodes.

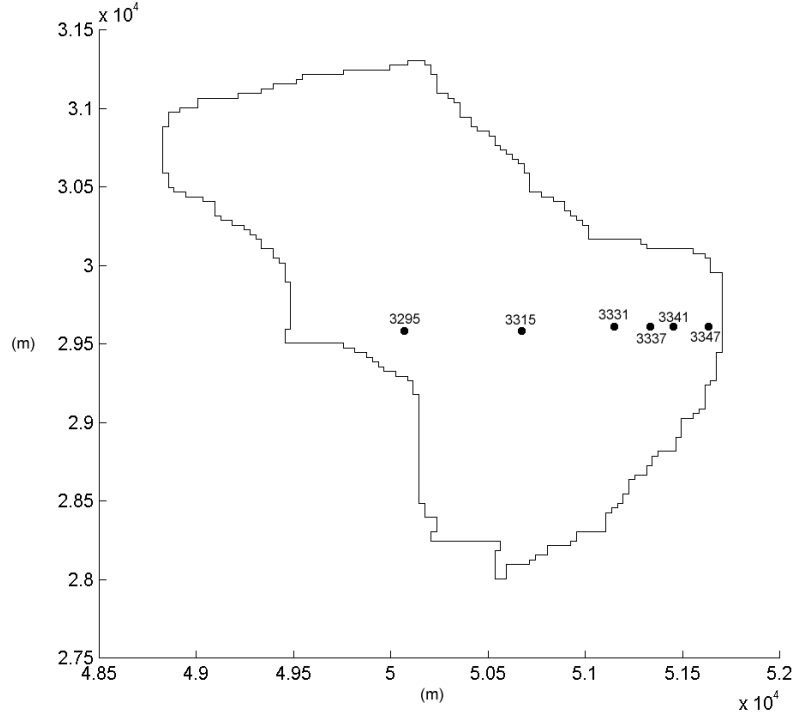


Figure 9: Location of selected surface nodes for vertical profile output

## 6 Model simulations

### 6.1 Preliminary simulations

In order to get acquainted with the CATHY model and to determine the appropriate parameter settings, preliminary simulations were performed using only the FLOW3D module (i.e., no surface routing). Most of these simulations terminated before the end of the 240-day period due to numerical oscillations and back stepping. The mass balance errors for these simulations were very large.

The simulations started with a fully saturated vertical hydrostatic profile and during the simulations there was no atmospheric input. The object of these simulations was to drain the catchment and examine the behavior of the CATHY model and the effect of various numerical discretization and solution options (mass lumping, implicit time stepping, convergence tolerances, Dirichlet and seepage face boundary conditions, soil characteristics, vertical layering, etc.).

The slopes of the Brisy subcatchment become steeper towards the outlet in the south. With a fully saturated vertical hydrostatic profile and no routing of the water, very large pressure heads will build up at the surface of the steeper slopes. A simulation was tried with only half of the soil saturated and with a vertical hydrostatic profile, giving better but still unsatisfactory results. For further simulations it was thus decided that surface routing had to be taken into account and the coupled model, including SURF\_ROUTE, should be used.

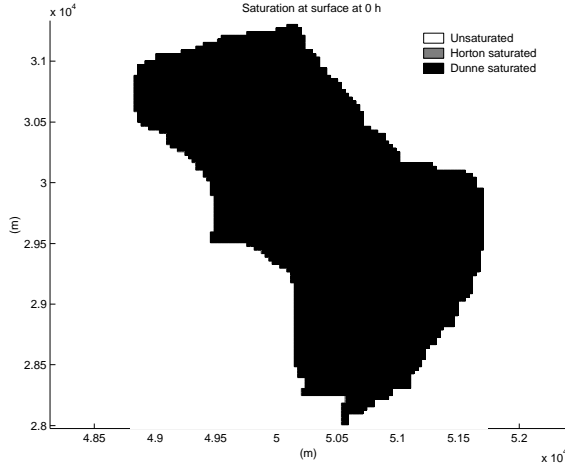


Figure 10: 10-day evaporation simulation: saturation at surface at  $t=0h$

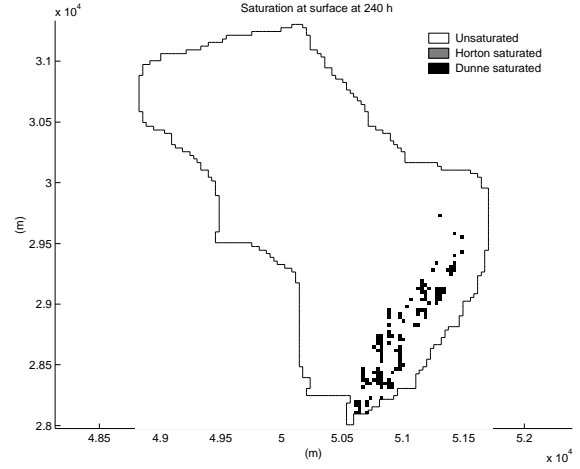


Figure 11: 10-day evaporation simulation: saturation at surface at  $t=240h$

## 6.2 Simulation to generate initial conditions

To generate initial pressure heads for the simulation of the 240-day storm-interstorm period, a 10-day drainage simulation was performed starting from fully saturated vertical hydrostatic conditions and applying a constant evaporation rate of 6 mm/day for the entire 10-day period. The intention was to establish “reasonable” starting conditions for the subsequent storm-interstorm simulation, in the sense of having a partially saturated subcatchment (the period immediately preceding the selected 240-day sequence is of relatively low rainfall) with a pressure head distribution that is adapted to the topographic and other features of the subcatchment. The simulation results for this 10-day drydown period are shown in Figures 10–17.

### 6.2.1 A note on post-processing

The output data of the CATHY model is structured in a series of ASCII files corresponding to various primary and derived fields distributed in space and time. The primary output field is pressure head, and from this field the model also computes moisture content (water saturation), water table depth, relative conductivity, and groundwater velocity. All these fields can be output at user-specified simulation times and as 3D, 2D (surface), and 1D (vertical profile) outputs. All post-processing was done in MATLAB using scripts specially written to read in the output data from CATHY and generate graphics.

## 6.3 240-day storm-interstorm simulation

The model and grid setup for the 240-day storm-interstorm period was the same as for the 10-day evaporation simulation. The atmospheric input was given as a histogram derived from Figure 8. Further parameter settings are given below, and the simulation results are shown in Figures 18–43.

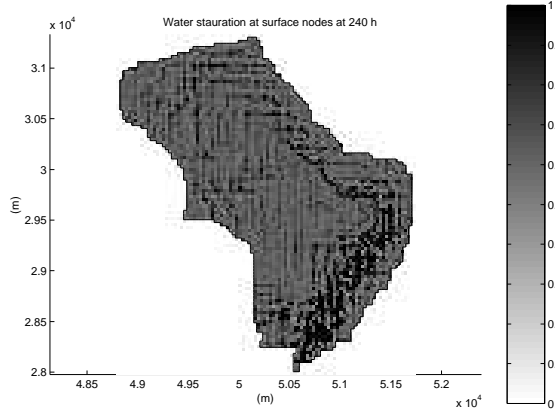


Figure 12: 10-day evaporation simulation: water saturation at surface at  $t=240h$

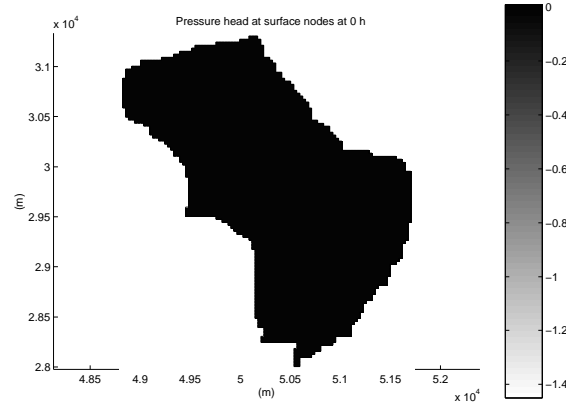


Figure 13: 10-day evaporation simulation: pressure head (m) at surface nodes  $t=0h$

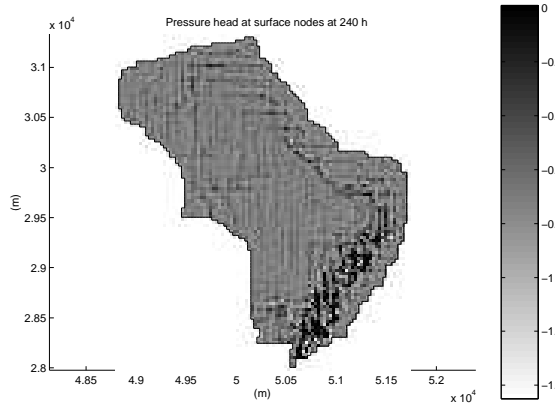


Figure 14: 10-day evaporation simulation: pressure head (m) at surface nodes  $t=240h$

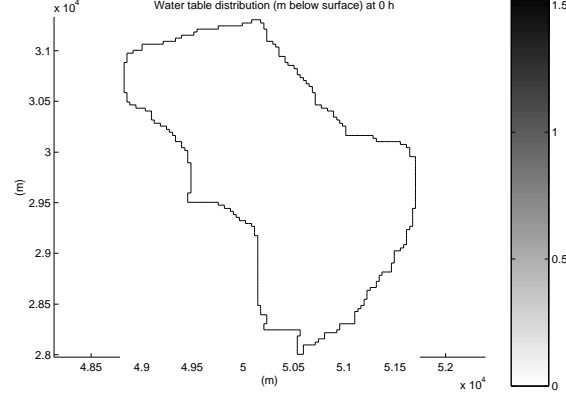


Figure 15: 10-day evaporation simulation: water table distribution (m below surface) at  $t=0h$

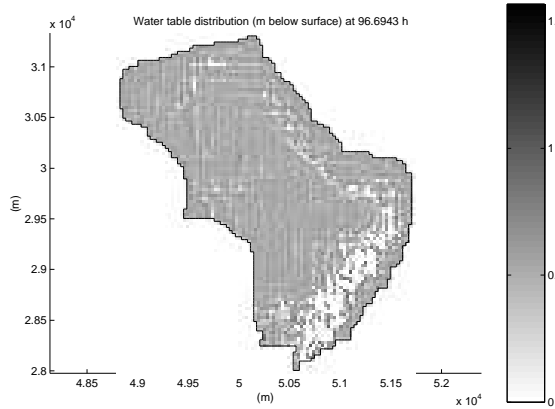


Figure 16: 10-day evaporation simulation: water table distribution (m below surface) at  $t=96h$

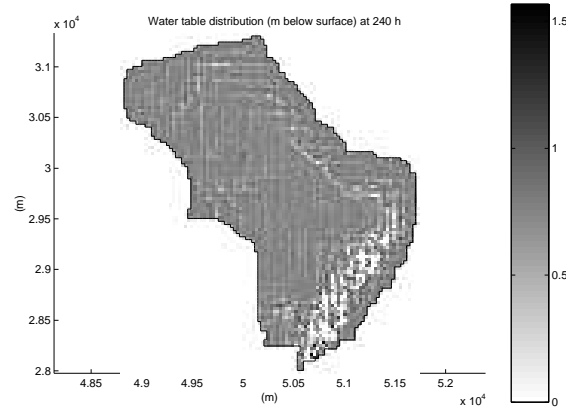


Figure 17: 10-day evaporation simulation: water table distribution (m below surface) at  $t=240h$

```

ISIMGR (0 FLOW3D only w/ grid input,
        1 FLOW3D only w/ DEM input,
        2 FLOW3D and SURF_ROUTE w/ DEM) =      2
PONDH_MIN (MIN. PONDING HEAD) =      1.00000E-02
IPRT1 (FOR OUTPUT OF INPUT DATA) =      2
IPRT (FOR ELEM VEL & DET NODAL OUTPUT)=      4
NPRT (# OF TIME VALUES FOR DET OUTPUT)= 239
NUMVP (# OF SURF NODES FOR VP OUTPUT) =      6
NR (# OF NODES FOR PARTIAL OUTPUT) =      0

KSLOPE (0 ANA, 1 KSL/ANA, 2 KSL/C-DIFF,
        3 LOC KSL/ANA, 4 LOC TAN-SLOPE) =      0
TOLKSL (TOLERANCE FOR CHORD SLOPE) =      1.00000E-02

ISFONE (0 ALL-NODE SFEX UPD, 1 1-NODE) =      1
ISFCVG (0 NL CONVG W/O SFEX, 1 W/ SFEX) =      0
TETAF (EG: 1 BACKWARD EULER, 0.5 C-N) =      5.00000E-01
LUMP (MASS LUMPING IF NONZERO) =      0
IOPT (1 PICARD, 2 NEWTON) =      1
NLRELX (0 NORELX,1 CONS RELX,2 VAR RELX)=      0
L2NORM (0 INFINITY NORM, ELSE L2 NORM) =      0
TOLUNS (TOLERANCE FOR NONLINEAR ITER) =      1.00000E-02
TOLSWI (TOLERANCE FOR BC SWITCHING) =      1.00000E+30
ERNLMX (MAX ALLOWABLE CVG OR RESID ERR) =      1.00000E+30
ITUNS (MAX NONLINEAR ITER / TIME STEP) =      10
ITUNS1 (DELTAT INCREASE THRESHOLD) =      5
ITUNS2 (DELTAT DECREASE THRESHOLD) =      8

ISOLV (-5 BiCGSTAB w/ diag precondition,
        -4 BiCGSTAB without precondition,
        -3 TFQMR w/ diag precondition,
        -2 TFQMR without precondition,
        -1 TFQMR w/ K^-1 precondition,
        0 BiCGSTAB w/ K^-1 precondition,
        1 GRAMRB (min residual),
        2 GCRK(5) (ORTHOMIN),
        3 NONSYM (direct solver)) =      0
ITMXCG (MAX ITER FOR CG LINEAR SOLVERS) =      500
TOLCG (TOLER. FOR CG LINEAR SOLVERS) =      1.00000E-10

DELTAT (INITIAL TIME STEP SIZE) =      1.00000E-03
DTMIN (MINIMUM TIME STEP SIZE) =      1.00000E-06
DTMAX (MAXIMUM TIME STEP SIZE) =      2.00000E+00
TMAX (TIME AT END OF SIMULATION) =      5.76000E+03
DTMAGA (MAG. FACTOR FOR DELTAT, ADD.) =      0.00000E+00
DTMAGM (MAG. FACTOR FOR DELTAT, MULT.) =      1.03000E+00
DTREDS (RED. FACTOR FOR DELTAT, SUB.) =      0.00000E+00
DTREDM (RED. FACTOR FOR DELTAT, MULT.) =      7.50000E-01

INITIAL PRESSURE HEAD
  1 -7.607E-01    2 -7.626E-01    3 -8.426E-01    4 -5.889E-01
  5 -7.436E-01    6 -8.154E-01    7 -5.899E-01    8 -7.639E-01
  9 -7.476E-01   10 -5.627E-01   11 -7.611E-01   12 -8.115E-01
 13 -7.890E-01   14 -8.161E-01   15 -7.920E-01   16 -8.293E-01
 17 -8.274E-01   18 -8.060E-01   19 -8.546E-01   20 -7.278E-01
    .
    .
    .
37565  2.536E+00 37566  2.264E+00 37567  2.825E+00 37568  2.784E+00

```

37569	1.836E+00	37570	1.372E+00	37571	1.298E+00	37572	2.486E+00
37573	2.617E+00	37574	2.991E+00	37575	2.900E+00	37576	2.779E+00
37577	2.466E+00	37578	2.345E+00	37579	2.254E+00	37580	2.334E+00
37581	2.275E+00	37582	2.298E+00	37583	2.260E+00		

```

PMIN (AIR DRY PRESSURE HEAD VALUE) = -9.99999E+04
IVGHU (0 van Genuchten,
      1 extended van Genuchten,
      2 Huyakorn with Kr=Se**n,
      3 Huyakorn with log_10 Kr(Se),
      4 Brooks-Corey) = 4
BCBETA = 1.20000E+00
BCRMC = 6.00000E-02
BCPSAT = -4.50000E-01

```

SATURATED HYDRAULIC CONDUCTIVITY, SPECIFIC STORAGE, AND POROSITY VALUES						
LAYER	MAT.TYPE	X-PERM	Y-PERM	Z-PERM	STORAGE	POROSITY
1	1	2.50000E-02	2.50000E-02	2.50000E-02	1.60000E-02	4.50000E-01
2	1	2.50000E-02	2.50000E-02	2.50000E-02	1.60000E-02	4.50000E-01
3	1	2.50000E-02	2.50000E-02	2.50000E-02	1.60000E-02	4.50000E-01
4	1	3.71000E-03	3.71000E-03	3.71000E-03	1.60000E-02	4.90000E-01
5	1	3.71000E-03	3.71000E-03	3.71000E-03	1.60000E-02	4.90000E-01
6	1	3.71000E-03	3.71000E-03	3.71000E-03	1.60000E-02	4.90000E-01

```

NDIR (# OF NON-ATM, NON-SF DIR NODES 2D)= 0
NDIRC(# OF FIXED NATM,NSF DIR NODES 3-D)= 0
NP (TOTAL # OF NATM,NSF DIR NODES 3-D)= 0
NQ (# OF NON-ATM, NON-SF NEU NODES 3D)= 0
NSF (# OF SEEPAGE FACES) = 0
N (# OF NODES IN 3-D MESH) = 37583
NT (# OF TETRAHEDRA IN 3-D MESH) = 185616
NTERM (# OF NONZERO TERMS IN SYS. MAT.) = 273637
HSPATM(O SPAT. VAR. ATM BC, ELSE HOMO.) = 1

```

```

TIME STEP: 1 DELTAT: 1.0000E-03 TIME: 1.0000E-03
*****

```

```

LINEAR SOLVER CONVERGENCE BEHAVIOR
iter      residual    real residual
  8    3.885401E-11    3.885401E-11 <<SYMMETRIC SOLVER>>

```

```

NONLINEAR CONVERGENCE BEHAVIOR
iter- convergence error norms node PNEW at POLD at residual error norms
ation      PL2      PIKMAX IKMAX      IKMAX      IKMAX      FL2      FINF
  1  2.3149E-03  1.4524E-03 10149  2.43E-01  2.41E-01  1.465E+01  2.432E+00
CONVERGENCE ACHIEVED IN 1 ITERATIONS

```

```

INFLOW (I) AND OUTFLOW (O) FROM ATM (A) AND NON-ATM, NON-SEEP FACE (N) BC'S;
'C F' CURRENT FLUX; 'P F' PREVIOUS FLUX; 'VOL' VOLUME
IA DIRIC OA DIRIC IN DIRIC ON DIRIC IA NEUMN OA NEUMN IN NEUMN ON NEUMN
C F  0.0E+00  0.0E+00  0.0E+00  0.0E+00  0.0E+00  0.0E+00  0.0E+00  0.0E+00

```

P F	0.0E+00	0.0E+00	0.0E+00	0.0E+00	0.0E+00	0.0E+00	0.0E+00	0.0E+00
VOL	0.0E+00	0.0E+00	0.0E+00	0.0E+00	0.0E+00	0.0E+00	0.0E+00	0.0E+00

TOTAL I VOL	TOTAL O VOL	STOR CHNG VOL		ABS MASS BAL ERR	REL MASS BAL ERR,%
0.000E+00	0.000E+00	-8.55085E-02		8.55084941E-02	0.000000000E+00

```

TIME STEP:      2      DELTAT:   1.0300E-03      TIME:    2.0300E-03
*****
.
.
.

```

Figures 18, 26 and 30 are identical to Figures 10, 13 and 15 since the 10-day evaporation simulation generated the initial conditions for the 240-day storm-interstorm simulation. Figures 19, 23, 27 and 31 give the output at  $t=2160\text{h}$  (90 days, 1st of May). From Figure 8 it can be seen that this is after a relatively dry period. Compared to  $t=0$  the pressure head at the surface in the Brisys subcatchment has decreased (Figure 27), the surface is less saturated (Figure 19 and 23), and the water table has dropped (Figure 31). These figures also show that the water is more concentrated in the river Brisys. Figure 20 shows the saturation at the surface at  $t=4321\text{h}$  (180 days, 30 July). From Figure 8 it is shown that this is after a period with relatively high rainfall, but also with high evapotranspiration rates. Compared to Figure 19 ( $t=2160\text{h}$ ) more of the surface is saturated. Figures 24 and 28 give the saturation at the surface and the pressure head at the surface (m) at  $t=4321\text{h}$ . These figures also appear wetter than at the earlier time (Figures 23 and 27,  $t=2160\text{h}$ ). Compared to  $t=2160\text{h}$  the water table has dropped slightly but saturation along the river Brisys is even more pronounced (Figure 32). Figures 21, 25, 29 and 33 give the output for  $t=5760\text{h}$  (240 days, 2 October). These figures do not vary much from Figures 20, 24, 28 and 32 ( $t=4321\text{h}$ ).

Figures 34–39 give the vertical profile of pressure head at different locations (see Figure 9 for the selected transect). Nodes 3295, 3315 and 3331 are located on the west bank of the river Brisys, nodes 3341 and 3347 on the east bank, and node 3337 is located within the river itself. Figures 34, 35, 36 and 39 show an identical pattern with high pressure after a period with little evapotranspiration and lower pressure after a period with higher evapotranspiration. It is interesting that for the nodes furthest from the stream (3295, 3315, 3331 and 3347) the vertical profiles change rapidly at early time while at later times ( $t=4321\text{h}$  and  $t=5760\text{h}$ ) the change in pressure head distribution is very small and is significant only near the surface. After about 180 days these “upslope” profiles have more or less become equilibrated with the imposed 240-day wet-and-dry cycle represented by the rainfall and evapotranspiration data for 1993. For the nodes closest to or at the stream (3337 and 3341), on the other hand, the response to the storm-interstorm forcing is slower at early times but faster at later times, most likely due to the discharge function of these “downslope” nodes in receiving, with some delay, water from upslope nodes.

Figures 40–43 show the groundwater velocities at  $t=0\text{h}$  and  $t=5760\text{h}$  for the top layer and the bottom layer. Groundwater velocities clearly increase towards the outlet of the Brisys subcatchment.

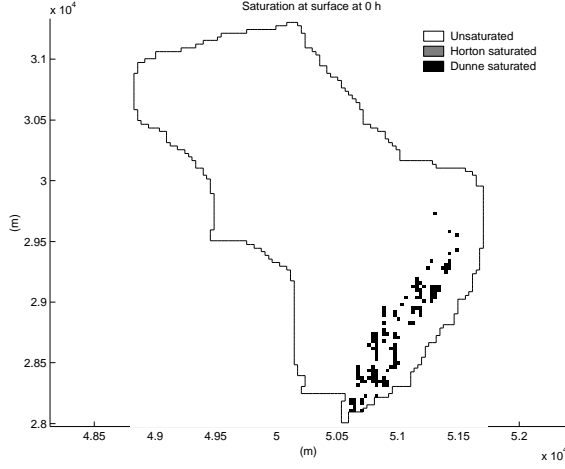


Figure 18: 240-day storm-interstorm simulation: saturation at surface at  $t=0h$

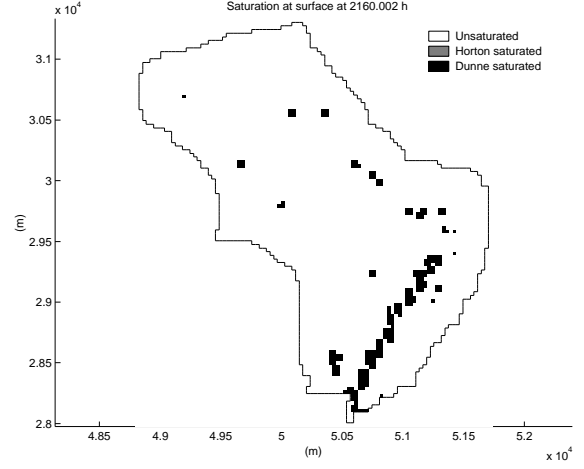


Figure 19: 240-day storm-interstorm simulation: saturation at surface at  $t=2160h$

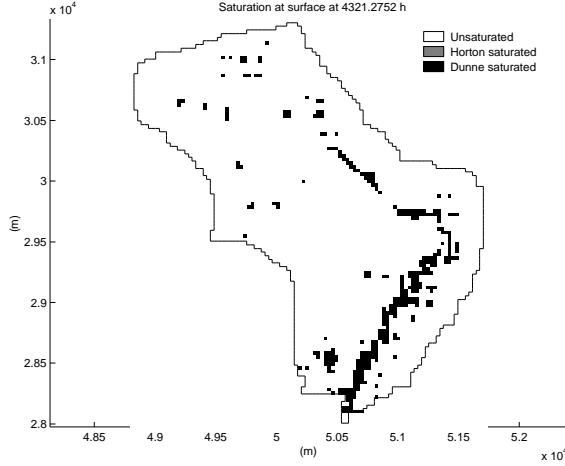


Figure 20: 240-day storm-interstorm simulation: saturation at surface at  $t=4321h$

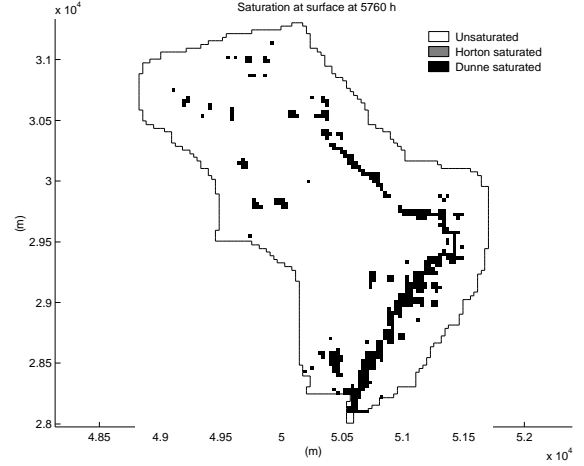


Figure 21: 240-day storm-interstorm simulation: saturation at surface at  $t=5760h$

## 7 Conclusions and recommendations

It can be concluded that for the 240-day storm-interstorm sequence the CATHY model performed a representative simulation that can be used as the basis of a synthetic dataset for model intercomparisons and for testing data assimilation methodologies. A closer analysis of the simulation results is needed to examine some small numerical anomalies such as the “black spots” (indicating unsaturated vertical profiles at these nodes) that appear in Figures 30–33 alongside the otherwise saturated channel of the Brisy river. These may be caused by numerical oscillations in the convergence of the model which are known to occur highly saturated conditions.

To improve the results of the simulation, more detailed soil data can be used, taking into account variations in soil depth and soil texture. According to the JRC dataset the soil depth is about 3 m and is fairly homogeneous over the Brisy subcatchment. More recent higher resolution data suggests that the soils in the upslope reaches of the catchment are much



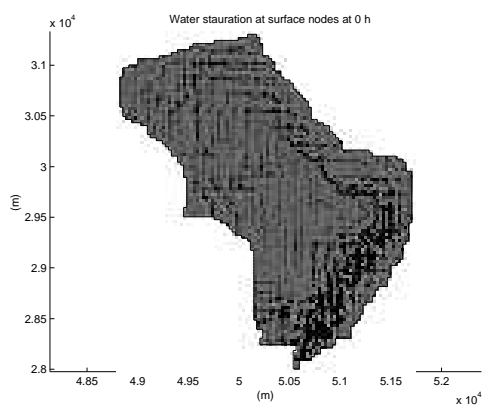


Figure 22: 240-day storm-interstorm simulation: water saturation at surface at  $t=0h$

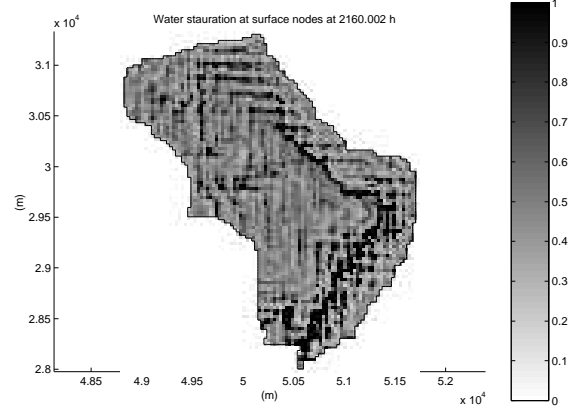


Figure 23: 240-day storm-interstorm simulation: water saturation at surface at  $t=2160h$

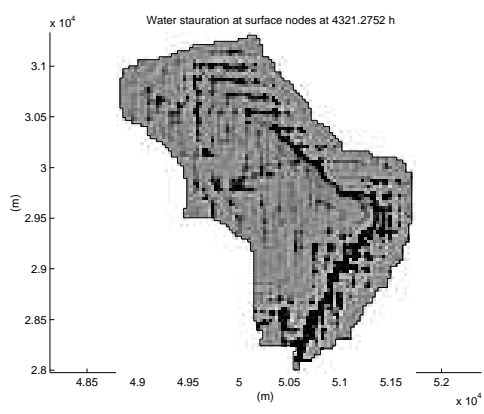


Figure 24: 240-day storm-interstorm simulation: water saturation at surface at  $t=4321h$

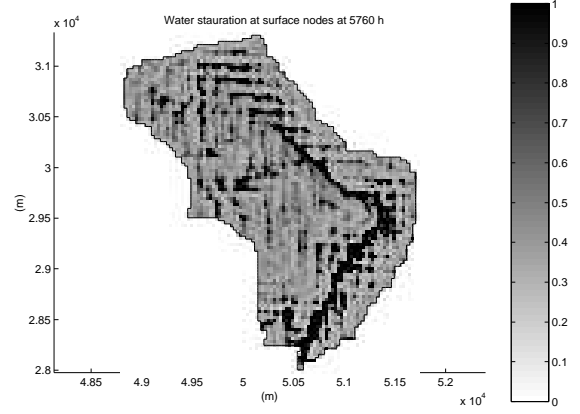


Figure 25: 240-day storm-interstorm simulation: water saturation at surface at  $t=5760h$

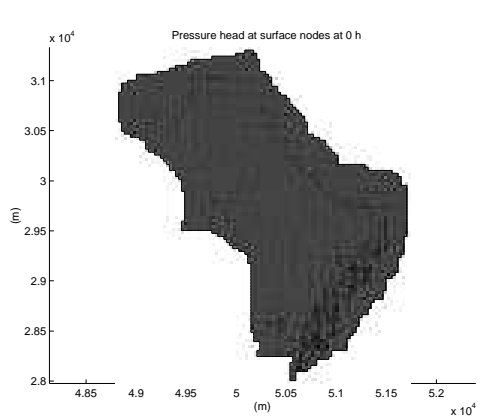


Figure 26: 240-day storm-interstorm simulation: pressure head (m) at surface nodes  $t=0h$

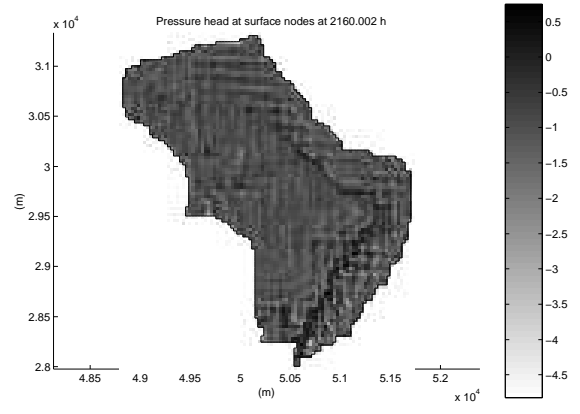


Figure 27: 240-day storm-interstorm simulation: pressure head (m) at surface nodes  $t=2160h$

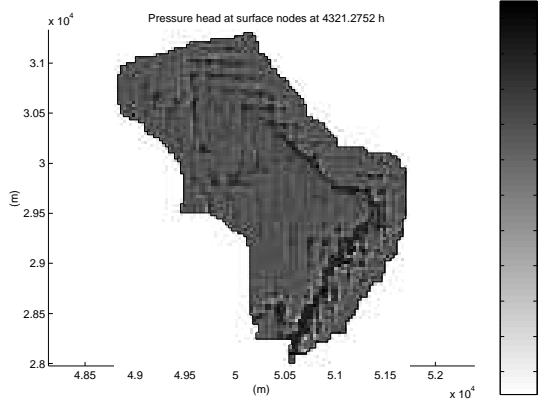


Figure 28: 240-day storm-interstorm simulation: pressure head (m) at surface nodes  $t=4321h$

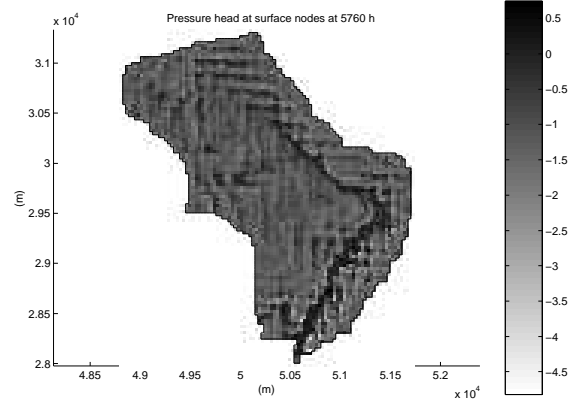


Figure 29: 240-day storm-interstorm simulation: pressure head (m) at surface nodes  $t=5760h$

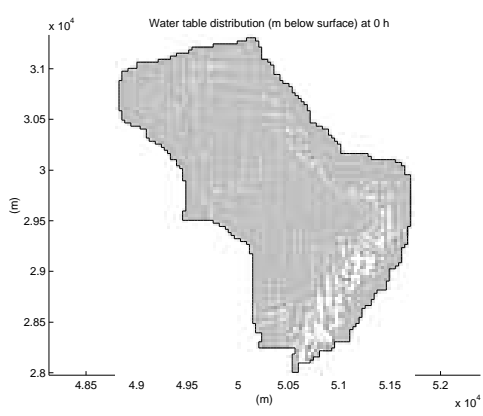


Figure 30: 240-day storm-interstorm simulation: water table distribution (m below surface) at  $t=0h$

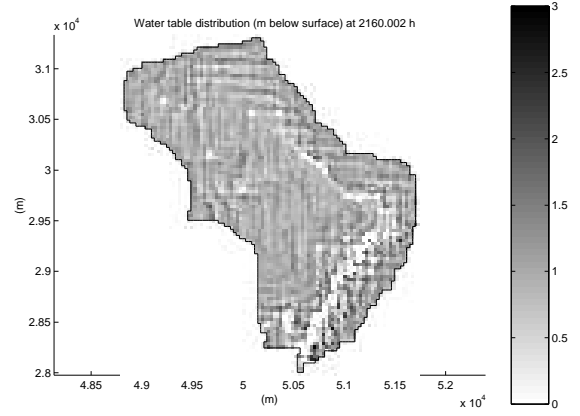


Figure 31: 240-day storm-interstorm simulation: water table distribution (m below surface) at  $t=2160h$

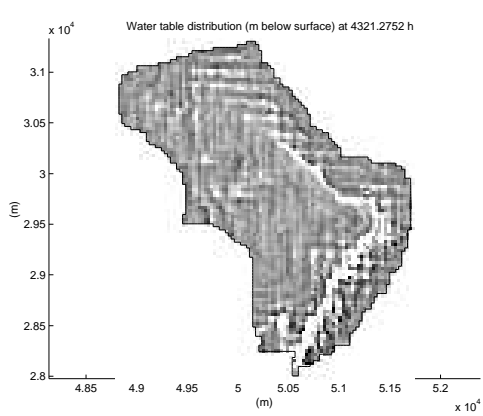


Figure 32: 240-day storm-interstorm simulation: water table distribution (m below surface) at  $t=4321h$

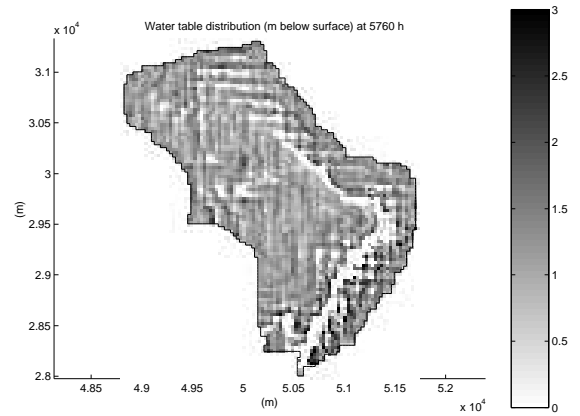


Figure 33: 240-day storm-interstorm simulation: water table distribution (m below surface) at  $t=5760h$

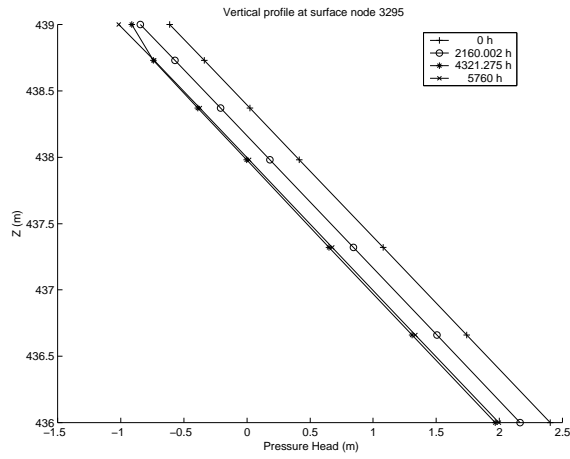


Figure 34: 240-day storm-interstorm simulation: vertical profile of pressure head at surface node 3295

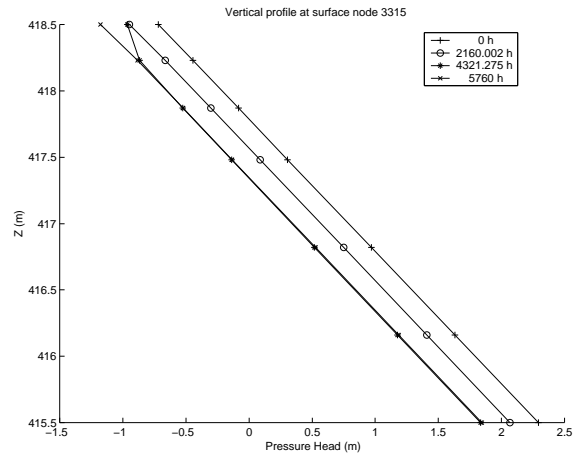


Figure 35: 240-day storm-interstorm simulation: vertical profile of pressure head at surface node 3315

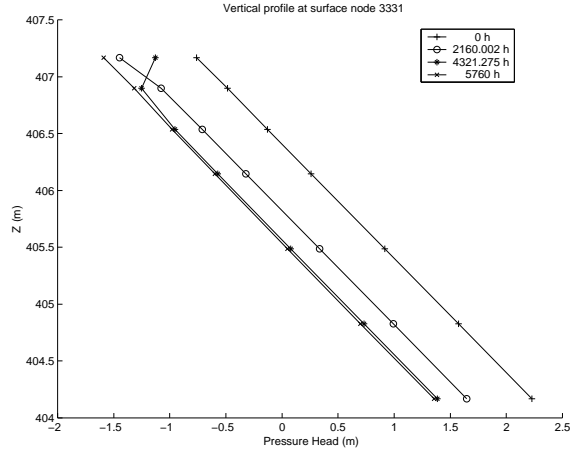


Figure 36: 240-day storm-interstorm simulation: vertical profile of pressure head at surface node 3331

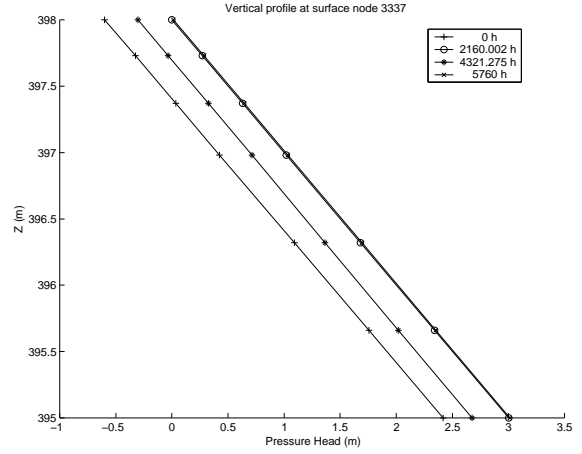


Figure 37: 240-day storm-interstorm simulation: vertical profile of pressure head at surface node 3337

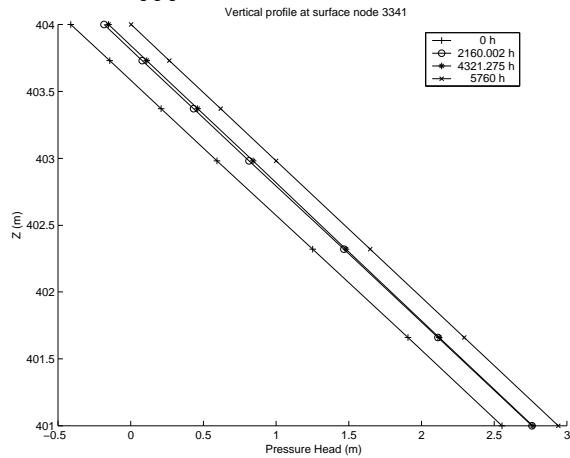


Figure 38: 240-day storm-interstorm simulation: vertical profile of pressure head at surface node 3341

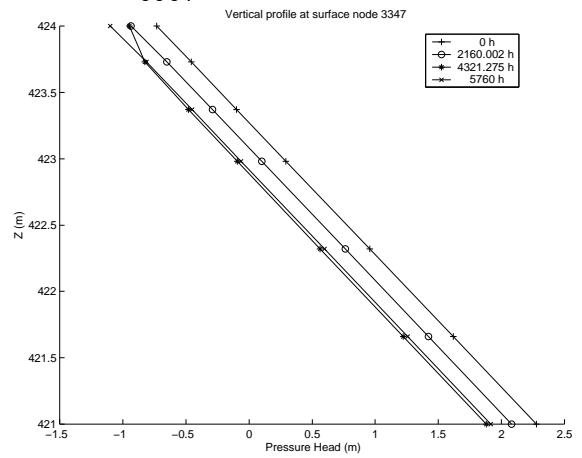


Figure 39: 240-day storm-interstorm simulation: vertical profile of pressure head at surface node 3347

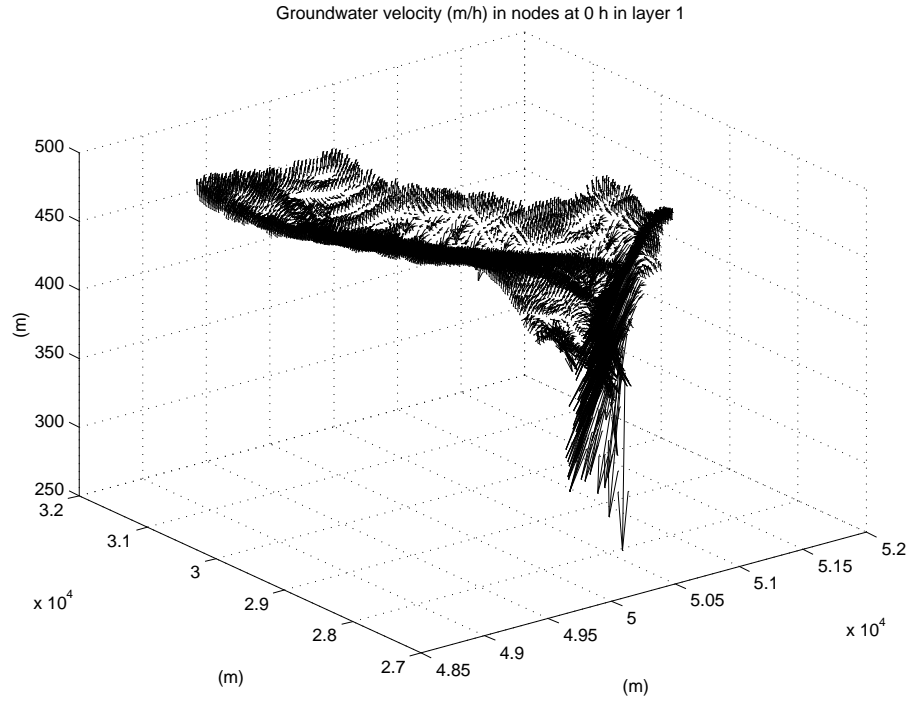


Figure 40: 240-day storm-interstorm simulation: groundwater velocity (m/h) at  $t=0$ h in layer 1

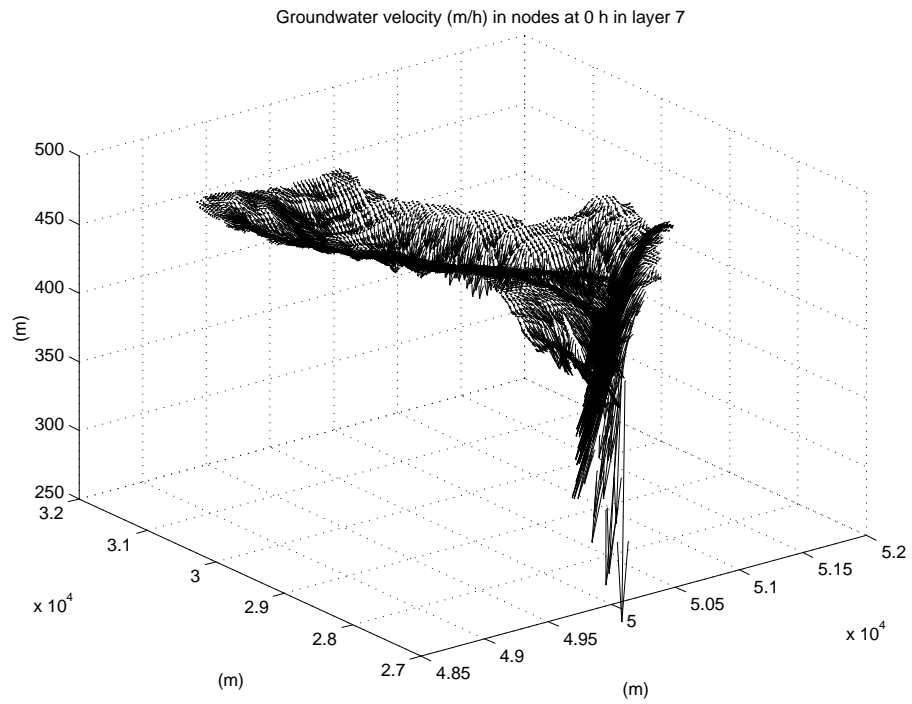


Figure 41: 240-day storm-interstorm simulation: groundwater velocity (m/h) at  $t=0$ h in layer 7

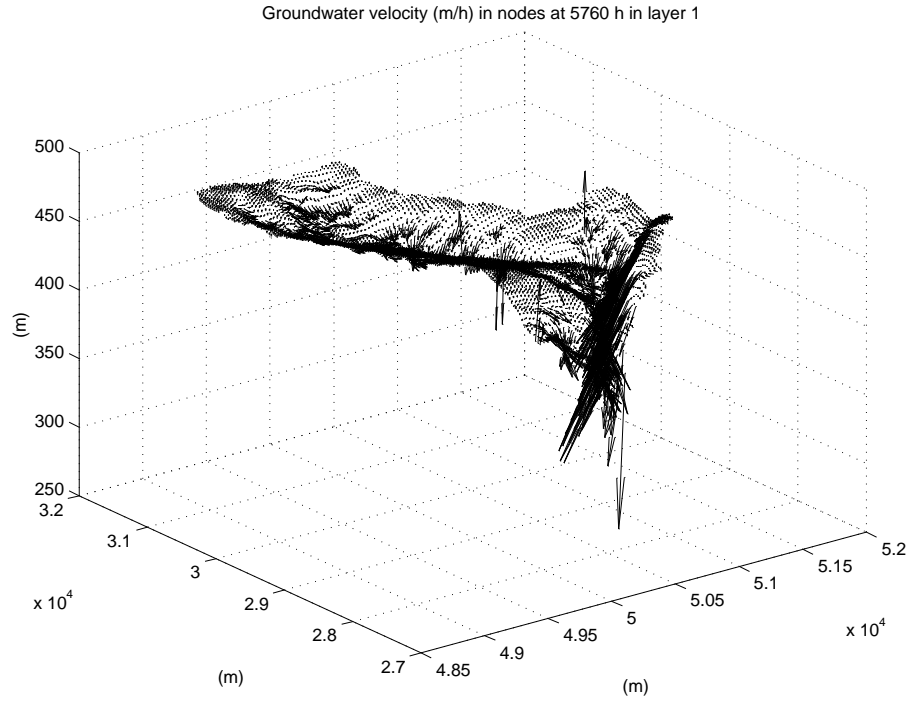


Figure 42: 240-day storm-interstorm simulation: groundwater velocity (m/h) at t=5760h in layer 1

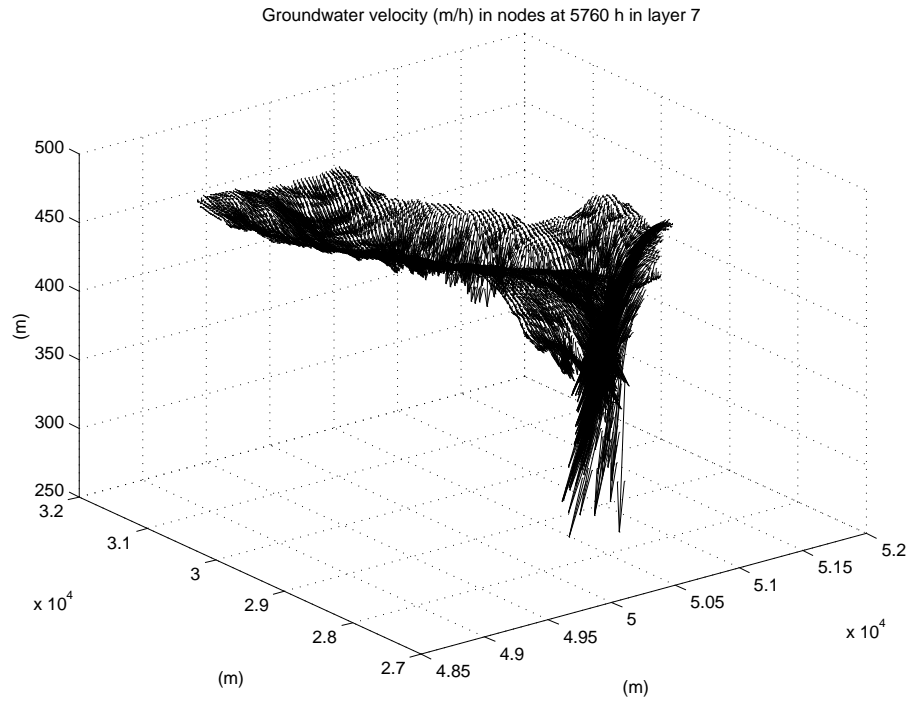


Figure 43: 240-day storm-interstorm simulation: groundwater velocity (m/h) at t=5760h in layer 7

thinner than the soils in the valleys.

The Brisy subcatchment is ungauged. Allowing that the objective of this study was to generate a synthetic dataset, it would nonetheless be interesting compare simulation results with a streamflow hydrograph. In this case a Dirichlet boundary condition will need to be imposed at the outlet node of the catchment.

**Acknowledgments** This work was funded by the Energy, Environment, and Sustainable Development Programme of the European Commission (contract EVK1-CT-1999-00022), and was performed as part of the first author’s student research stage at Wageningen University and Research Center, the Netherlands.

## References

- Bixio, A. C., S. Orlandini, C. Paniconi and M. Putti, Physically-based distributed model for coupled surface runoff and subsurface flow simulation at the catchment scale. In: Bentley, L. R. (ed.) *Computational Methods in Water Resources, Vol. 2*. Balkema, pp 1115–1122, 2000.
- de Roo, A. and G. Somma, DAUFIN project hydrological dataset for the Ourthe and Geer watersheds of the Meuse river basin. CD-ROM, Joint Research Center, Ispra, Italy, 2000.
- Leopold, L. B. and T. Maddock Jr., The hydraulic geometry of stream channels and some physiographic implications. Professional Paper 252, U.S. Geological Survey, Washington, DC, 1953.
- Montgomery, D. R. and E. Foufoula-Georgiou, Channel network source representation using digital elevation models, *Water Resour. Res.* 29(12), 3925–3934, 1993.
- Orlandini, S. and R. Rosso, Diffusion wave modeling of distributed catchment dynamics, *J. Hydrol. Engrg., ASCE* 1(3), 103–113, 1996.
- Orlandini, S. and R. Rosso, Parameterization of stream channel geometry in the distributed modeling of catchment dynamics, *Water Resour. Res.* 34(8), 1971–1985, 1998.
- Paniconi, C. and E. F. Wood, A detailed model for simulation of catchment scale subsurface hydrologic processes, *Water Resour. Res.* 29(6), 1601–1620, 1993.
- Paniconi, C. and M. Putti, A comparison of Picard and Newton iteration in the numerical solution of multidimensional variably saturated flow problems, *Water Resour. Res.* 30(12), 3357–3374, 1994.
- Roulin, E., DAUFIN project meteorological dataset for the Ourthe and Geer watersheds of the Meuse river basin. CD-ROM, Royal Meteorological Institute, Brussels, Belgium, 2000.